IACSIT International Journal of Engineering and Technology, Vol.2, No.6, December 2010
ISSN: 1793-8236

Speckle Filtering of Ultrasound B-Scan Images - A Comparative Study of Single Scale Spatial Adaptive Filters, Multiscale Filter and Diffusion Filters

[1]R. Sivakumar, Member IACSIT, [2]M. K. Gayathri and [3]D. Nedumaran, *Member IEEE, IACSIT*

***Abstract*- This paper presents a comparative study of among one Multi Scale filter (wavelet), nine single scale spatial adaptive filters (viz., Frost, Enhanced Frost, Median, Lee, Enhanced Lee, Kuan, Gamma Map, Wiener, Homomorphic speckle filters) and two Diffusion filters (viz., Speckle Reduction Anisotropic Diffusion (SRAD), Perona Malik Anistropic Diffusion (PMAD)) that are widely used for speckle noise reduction in biomedical ultrasound B-Scan images. The main objective of this study is to identify the efficient and optimum speckle filter in terms of preserving the edge details of the images with effective denoising. The performance of the filters are best estimated by calculating twenty-one established performance metrics along with execution time in order to determine the effective and optimum-despeckling algorithm for real time implementation. To do this, we have developed a cumulative speckle reduction (CSR) algorithm in the MATLAB environment, which performs all despeckle filtering functions as well as performance metrics calculation in a single trial. In the case of diffusion filter implementation, provision is given to execute the diffusion filter for several trials to identify the best iteration in terms of denoising the speckle and preserving the diagnostic information found in the B-scan images. The algorithm has been experimented with more than 200 digital ultrasound B-scan images of kidney, abdomen, liver and choroids. Based on the visual inspection of the despeckled images and the calculation of the performance metrics, it is found that SRAD and Wavelet despeckling filters are exhibiting fairly well performance over the other standard spatial filters.**

***Index Terms*— Ultrasound B-Scan image, Speckle, Single Scale Spatial Adaptive Filters, Multiscale Filter, SRAD, Perona Malik (PMAD) Filter, Performance Metrics**

I. INTRODUCTION

Medical ultrasound B-scan imaging has been used for effective diagnostics of diseases over the past decades due to its noninvasive, harmless, portable, accurate and cost-effective characteristics [1-5]. Unfortunately, Ultrasound images are degraded by an intrinsic artifact called speckle, which is the result of the constructive and destructive coherent summation of ultrasound echoes. Especially, speckle noise occurs in the images of soft organs such as liver and kidney whose underlying structures are too small to be resolved by the large ultrasound wavelength. Several techniques have been developed to suppress the speckle and found in the literature describing the properties [6-8], modeling, analysis and filtering [9-14] of speckle noise in ultrasound images. This paper focuses on the speckle reduction techniques in ultrasound B-scan images. Several models of speckle noise have been proposed to perfect the despeckling filters, of which we have considered the following mathematical model [15] given in equation 1 for the analysis of speckle noise.

$$R(x,y) = N(x,y)\eta_M(x,y) + \eta_A(x,y) \quad (1)$$

where $R(x,y)$ is the real noisy image, $N(x,y)$ represents an unknown noise free image, $\eta_M(x,y)$ and $\eta_A(x,y)$ are multiplicative and additive noise respectively.

II. SPECKLE FILTERING TECHNIQUES

Over the years, several techniques have been proposed to despeckle ultrasound images [16]. There are two major classifications of speckle reduction filters viz., compounding method and post acquisition method [17]. Compounding method can improve the target detectability but they suffer from degradation of spatial resolution and increased system complexity due to hardware modification. On the other hand, post acquisition methods include single scale spatial adaptive filtering methods and multiscale methods do not require any hardware modification, but improve the image details and reduce the speckle noise considerably through algorithm implementation. This paper presents the performance of the spatial adaptive filtering methods, anisotropic diffusion filtering methods and multiscale wavelet method in removing the speckle noise and preserving the diagnostics information in ultrasound B-scan images.

A. Single Scale Spatial Adaptive Filtering

Single scale spatial adaptive filter is based on the ratio of local statistics, which improves smoothing in homogenous regions of the B-scan images where speckle is fully developed and reduces appreciably in the other regions of the image in order to preserve the useful details of the image [17]. Spatial filters like Lee, and Kuan filter were the earliest filters working directly on the intensity of the image using local statistics [12-14]. Also, computation of local statistics, region growing procedure and application of smoothening operator are the three main steps involved in the implementation of single scale spatial adaptive speckle filtering [9]. This section describes the brief definition and mathematical description of the single scale spatial adaptive

Central Instrumentation & Service Laboratory, University of Madras, Guindy Campus, Chennai, India
E-mail: [3]dnmaran@gmail.com, [1]pambansiva@gmail.com

filters.

1) Frost filter: The Frost filter is an adaptive and exponentially weighted averaging filter based on the coefficient of variation, which is the ratio of the local standard deviation to the local mean of the degraded image [18]. It replaces the pixel of interest with a weighted sum of the values within the moving kernel and the weighting factors decrease with distance and increase with the increase in variance of the kernel. The resulting filter after some simplifications is given in equation 2.

$$W(x,y) = e^{-kC_I^2(x',y')|(x,y)|} \tag{2}$$

where k is a constant controlling the damping rate of the impulse response function, and (x',y') denotes the pixel to be filtered. It is seen that when the variation coefficient $C_I(x',y')$ is small, the filter behaves like an Low Pass filter smoothing out the speckles, and when $C_I(x',y')$ is large it has a tendency to preserve the original observed image.

2) Lee and Kuan filter: The Lee [12, 13] and Kuan [14] filter are based on the minimum mean square error (MMSE), which produce the speckle free image governed by the relationship given in equation 3 [19].

$$U(x,y) = I(x,y)W(x,y) + I'(x,y)(1 - W(x,y)) \tag{3}$$

where I' is the mean value of the intensity within the filter window, and *W(x,y)* is the adaptive filter coefficient calculated using the following formula.

$$W(x,y) = 1 - \frac{C_B^2}{C_I^2 + C_B^2} \quad \text{for Lee filter} \tag{4}$$

$$W(x,y) = \frac{1 - C_B^2 / C_I^2}{1 + C_B^2} \quad \text{for Kuan filter} \tag{5}$$

where C_I is the coefficient of variation of the noised image and C_B is the coefficient of variation of the noise. In general, the value of *W(x,y)* approaches zero in uniform areas, i.e., it approaches unity at edges which results in little modification of pixel values near edges.

3) Enhanced Frost and Enhanced Lee filter: According to Lopes et al, the ultrasound B-Scan images can be divided into the three classes based on the variation coefficients, C_B and C_I [18, 20]. The first class corresponds to the homogeneous areas in which the speckles may be eliminated simply by applying a Low Pass filter. The second class corresponds to the heterogeneous areas in which the speckles are to be reduced while preserving texture. And the third class includes areas containing isolated point targets, which should preserve the observed value. Based on the above considerations, the modified form of the Frost and the Lee filter functions are evaluated and are given in equations 6 and 8.

a) Enhanced Frost Filter:

$$W(x,y) = e^{-k\,func(C_I(x',y'))|(x,y)|} \tag{6}$$

where $func(C_I(x',y'))$ is a hyperbolic function of $C_I(x',y')$ defined as follows:

$$func(C_I) = \begin{cases} 0 & for\ C_I(x',y') < C_B \\ \dfrac{[C_I(x',y') - C_B]}{[C_{\max} - C_I(x',y')]} & for\ C_B \le C_I(x',y') \le C_{\max} \\ \infty & for\ C_I(x',y') > C_{\max} \end{cases} \tag{7}$$

b) Enhanced Lee Filter:

$$U(x',y') = \begin{cases} I'(x',y') & for\ C_I(x',y') \le C_B \\ I(x',y')W(x',y') + I'(x',y')(1 - W(x',y')) & for\ C_B < C_I(x',y') < C_{\max} \\ I(x',y') & for\ C_I(x',y') \ge C_{\max} \end{cases} \tag{8}$$

where

$$W(x',y') = \exp[-k(C_I(x',y') - C_B)/(C_{\max} - C_I(x',y'))]$$

Lopes et al also demonstrated that these modified filters are forced to achieve average value and observed value for the homogenous and isolated point target classes respectively, without filtering, in comparison with the original filters. Between these two extremes, the heterogeneous class exists, for which the modified filters have the similar forms as the original filters, but the filter responses are exaggerated due to the introduction of a hyperbolic function, which satisfied the condition that the more heterogeneous area is less smoothed [20].

4) Median filter: The median filter [21] is a spatial non-linear filter which removes pulse or spike noise by replacing the middle pixel value in the window with the median value of its neighbors in the window.

5) Gamma Map filter: Kuan et al [14] proposed a speckle reduction filter based on the application of maximum *a posteriori* (MAP) approach, which required the *a priori* knowledge of the probability density function (PDF) of the image. Lopes et al [20] modified the Kuan MAP filter by assuming a gamma distributed image and setting up two thresholds, since Kuan MAP filter assumed a Gaussian distribution for image reflectivity, which results in negative reflectivity. The Gamma MAP filter is given by the equation 9.

$$U(x',y') = \begin{cases} I'(x',y') & for\ C_I(x',y') < C_B \\ \dfrac{(\alpha - L - 1)I'(x',y') + \sqrt{I'^2(x',y')(\alpha - L - 1) + 4\alpha L I'(x',y')}}{2\alpha} & for\ C_B \le C_I(x',y') \le C_{\max} \\ I(x',y') & for\ C_I(x',y') > C_{\max} \end{cases} \tag{9}$$

Where L is the Number of Looks, $C_{\max}(x',y') = \sqrt{2C_B}$

$$and\ \alpha = \frac{1 + C_B^2}{C_I^2(x',y') - C_B^2}$$

6) Wiener filter: Wiener filtering is a method [15, 22] of restoring images in the presence of blur as well as noise. Wiener filter performs smoothing of the image based on the computation of local image variance. When the local variance of the image is large, the smoothing is little. On the other hand, if the variance is small, the smoothing will be better. This approach often produces better quality results than linear filtering, since the Wiener filtering is adaptive, more selective than a comparable linear filter. It preserves edges and other high-frequency information of the image, but requires more computation time than linear filtering.

7) Homomorphic Filtering: Homomorphic filtering performs image enhancement by applying the filter function and inverse FFT on the logarithmic compressed image [23]. The filter function *H(u,v)*, may be constructed using either the band-pass or the high-boost Butter worth filter. In this study, the high-boost Butterworth technique has been employed and is given in equation 10

$$H_{u,v} = \delta_L + \frac{\delta_H}{1+\left(\frac{D_0}{D_{u,v}}\right)^2} \tag{10}$$

$$D_{u,v} = \sqrt{(u-N/2)^2 2+(v-N/2)^2} \tag{11}$$

where D_0 is the cut of frequency of the filter, δ_L is the low frequency gain, δ_H is the high frequency gain, u and v are the spatial coordinates of the frequency transformed image and *N* is the dimensions of the image in the u and v space.

B. Multi scale Filtering:

Mallat invented the Multiscale analysis concept for image processing applications, which can be viewed as a successive approximation or successive refinement of a signal and is closely related with the wavelet transform [24][25][26]. From the signal $f_2^{j+1}(x)$, two discrete signals $f_2^j(x)$ (approximate $f(x)$ at resolution 2^j) and d_2^j (information content lost between higher resolution 2^{j+1} and lower resolution 2^j) can be computed as

$$f_{2^j}(x) = \sum_{n=-\infty}^{n=\infty} f_{2^{j+1}}(x)\tilde{h}_0(2x-n) \tag{12}$$

$$d_{2^j}(x) = \sum_{n=-\infty}^{n=\infty} f_{2^{j+1}}(x)\tilde{h}_1(2x-n) \tag{13}$$

where $\tilde{h}_0(n) = h_0(-n), \tilde{h}_1(n) = h_1(-n)$ and $f_{2^0}(x) = f(x)$

This decomposition is equivalent to passing the signal $f_{2^j}(x)$ through a pair of low pass and high pass filters $\tilde{h}_0(n)$ and $\tilde{h}_1(n)$, followed by the sub sampling with a factor two.

Separable 2D Discrete Wavelet Transform (DWT): The wavelet transform can be generalized to any dimension. In the particular case of separable multiscale approximation, the two dimensional scaling function Φ(x,y) can be expressed as the product of two one dimension scaling function *(ϕ(x), ϕ(y*

$$\Phi(x,y) = \phi(x)\phi(y) \tag{14}$$

and the 2D Wavelet function can be expressed as separable product of scale function ϕ and wavelet function ψ as;

$$\begin{aligned} \psi_1(x,y) &= \phi(x)\psi(y) \\ \psi_2(x,y) &= \psi(x)\phi(y) \\ \psi_3(x,y) &= \psi(x)\phi(y) \end{aligned} \tag{15}$$

The corresponding filter equations to implement 2D DWT are:

$$\begin{aligned} h_{LL}(k,v) &= h(k)h(v), h_{LH}(k,v) = h(k)g(v) \\ h_{HL}(k,v) &= g(k)h(v), h_{HH}(k,v) = g(k)g(v) \end{aligned} \tag{16}$$

Where the subscripts L and H denote the low pass and high pass filter characteristic in the horizontal (k) and vertical direction (v), receptively. The Multiscale analysis of the ultrasound image can be explained based on the wavelet decomposition [11] described in this section. The main aim of this method is to improve the ultrasound image quality of subjective visualization. The multiscale analysis of wavelet based speckle reduction process usually include (1) logarithmic transformation (2) Discrete wavelet transformation (3-level decompositions) (3) Thresholding the wavelet coefficients (Threshold may be universal or sub band adaptive) (4) inverse discrete wavelet transform and (5) exponential transformation. The schematic block diagram of the multiscale analysis of speckle reduction method and the results of the sub-band images of the 2D-Wavelet transform are shown in fig.1 and fig.2, respectively.

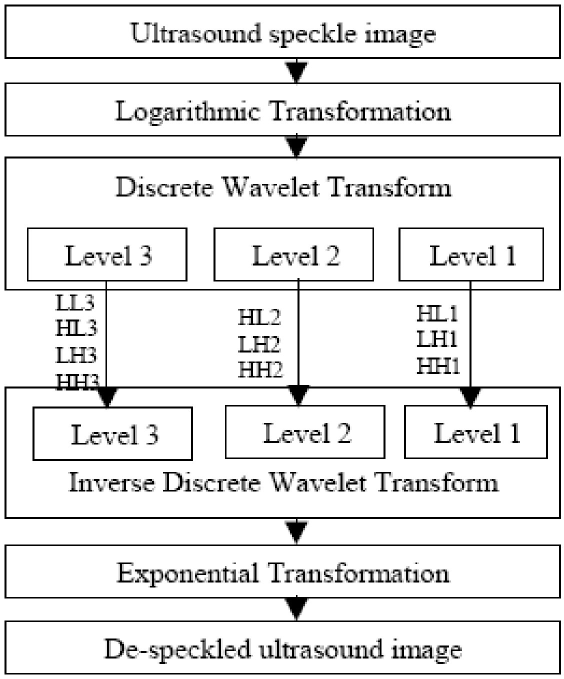

Fig.1 Block diagram of the multiscale wavelet analysis

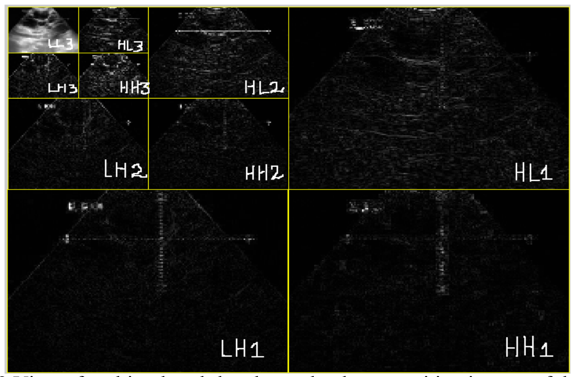

Fig.2 View of multiscale sub-band wavelet decomposition images of the ultrasound B-scan (kidney) image

C. Diffusion Filtering

Diffusion filters may be applied directly on the image for removing the speckle noise by solving partial differential equation. An Anisotropic diffusion performs contrast enhancement and noise reduction without requiring the power spectrum information of the image [20]. In this work, two diffusion filters have been attempted and their descriptions are given here.

1) SRAD filter: Speckle Reducing Anisotropic Diffusion (SRAD) [27] filter eliminates speckle without distorting and destroying useful image information and important image edges [28], respectively. The SRAD exploits the instantaneous coefficient variation in reducing the speckle.

2) Anistropic Diffusion filter: In this study, Perona and Malik [29-31] Anistropic Diffusion (PMAD) method based on the nonlinear partial differential equation (PDE) is used and its mathematical functions are given in equation 17 and 18.

$$\frac{\partial I}{\partial t} = div\left[c\left(|\nabla I|\right)\cdot \nabla I\right] \quad (17)$$

$$I(t=0) = I_0 \quad (18)$$

where ∇ is the gradient operator, the 'div' divergence operator, | | denotes the magnitude, c(x) is the diffusion coefficient, and I_0 the initial image. They suggested two diffusion coefficients, which are given in equations 19 and 20.

$$c(x) = \frac{1}{1+\left(\frac{x}{k}\right)^2} \quad (19)$$

and

$$c(x) = \exp\left[-\left(\frac{x}{k}\right)^2\right] \quad (20)$$

where k is an edge magnitude parameter. In this method, the image edge or boundary can be detected using gradient magnitude. A discrete form of the equation (17) is given by

$$I_s^{t+\Delta t} = I_s^t + \frac{\Delta t}{|\bar{\eta}_s|}\sum_{p\in\bar{\eta}_s} c\left(\nabla I_{s,p}^t\right)\nabla I_{s,p}^t \quad (21)$$

Where I_s^t is the sampled image, s is the pixel position in a discrete two-dimensional (2-D) grid, and Δt is the time step size, $\bar{\eta}_s$ represents the spatial neighborhood of pixel s, $|\bar{\eta}_s|$ is the number of pixels in the window, and $\nabla I_{s,p}^t = I_p^t - I_s^t, \forall p \in \bar{\eta}_s$.

III. Parameters/Metrics for Analyzing Despeckle Filter Performance

To quantify the performance of the Despeckle filter algorithm in terms of the efficiency of speckle noise reduction and enhancing the useful image information, the following established performance metrics found in the literatures [27] [32-46] are calculated in this study and their mathematical expression, significance, etc are given in Table I

TABLE I Performance metrics and their mathematical definitions

Performance Metrics	Mathematical Expression	Purpose
Average Difference (AD)	$AD = \frac{1}{MN}\sum_{j=1}^{M}\sum_{k=1}^{N}\left\|(X_{j,k} - X'_{j,k})\right\|$	Measures the average difference value between a particular pixel in the original and denoised images
Mean Square Error (MSE)	$MSE = \frac{1}{MN}\sum_{j=1}^{M}\sum_{k=1}^{N}(X_{j,k} - X'_{j,k})^2$	Quantify the amount of despeckling between the original and denoised images
Root Mean Square Error (RMSE)	$RMSE = \sqrt{\frac{1}{MN}\sum_{j=1}^{M}\sum_{k=1}^{N}(X_{j,k} - X'_{j,k})^2}$	Measure of square root of the squared error averaged over an pixel window
Peak Signal to Noise Ratio (PSNR)	$PSNR = 10\log_{10}\frac{(2^n-1)^n}{MSE} = 10\log_{10}\left(\frac{255^2}{MSE}\right)$	Provides the quality of the image in terms of the power of the original and denoised images.
Maximum Difference (MD)	$MD = Max(\left\|X_{j,k} - X'_{j,k}\right\|)$	Measure of the difference between the original and denoised images
Normalized Absolute Error (NAE)	$NAE = \frac{\sum_{j=1}^{M}\sum_{K=1}^{N}\left\|X_{j,k} - X'_{j,k}\right\|}{\sum_{j=1}^{M}\sum_{K=1}^{N}X_{j,k}}$	Measures the error prediction accuracy of the image
Normalized Mean Square Error (NMSE)	$NMSE = \frac{\sum_{j=1}^{M}\sum_{k=1}^{N}(X_{j,k} - X'_{j,k})}{\sum_{j=1}^{M}\sum_{k=1}^{N}X_{j,k}^2}$	Measure the variation of the Mean square Error
Signal to Noise Ratio (SNR)	$SNR = 10\log_{10}\frac{\sigma_g^2}{\sigma_e^2}$	Compares the level of desired signal with respect to the level of background noise.
Structural Content (SC)	$SC = \frac{\sum_{j=1}^{M}\sum_{K=1}^{N}X_{j,k}^2}{\sum_{j=1}^{M}\sum_{K=1}^{N}(X'_{j,k})^2}$	Measure of similarity between the original and denoised images
Coefficient of Correlation (CoC)	$CoC = \frac{\sum_{j=1}^{M}\sum_{K=1}^{N}(X'_{j,k} - \bar{X}'_{j,k})(X_{j,k} - \bar{X}_{j,k})}{\sqrt{\sum_{j=1}^{M}\sum_{K=1}^{N}(X'_{j,k} - \bar{X}'_{j,k})^2 \sum_{j=1}^{M}\sum_{K=1}^{N}(X_{j,k} - \bar{X}_{j,k})^2}}$	Indicates the strength and direction of linear relationship between the original and denoised images

Normalized Cross Correlation (NCC)	$NCC = \dfrac{\sum_{j=1}^{M}\sum_{K=1}^{N}(X_{j,k})(X'_{j,k})}{\sum_{j=1}^{M}\sum_{K=1}^{N}X_{j,k}^2}$	Measure of similarity between the original and denoised images
Image Quality Index (IQI)	$IQI = \dfrac{4\sigma_{xx'}\bar{X}\bar{X}'}{\left[\sigma_x^2+\sigma_{x'}^2\right]\left[\bar{X}^2+(\bar{X}')^2\right]}$	Represents the degree of distortion of the image in terms of loss of correlation, luminance distortion and contrast distortion. Distortion is less when IQI is equal to unity.
Contrast to Noise Ratio (CNR)	$CNR = \dfrac{\lvert\mu'-\mu''\rvert}{\sqrt{\sigma_1^2+\sigma_2^2}}$	Measure the contrast ratio of the image and the quality of the image.
Speckle Index (SI)	$SI = \dfrac{1}{MN}\sum_{j=1}^{M}\sum_{K=1}^{N}\dfrac{\sigma(X)}{\mu(X)}$	Measure of speckle removal in terms of average contrast of an image
Average Signal to Noise Ratio (ASNR)	$ASNR = \dfrac{1}{SI}$	Measures the average deviation of speckle noise with respect to mean value of the image.
Image Variance (IV)	$\sigma^2 = \dfrac{1}{MN}\sum_{j=1}^{M}\sum_{k=1}^{N}(X_{j,k}-\bar{X}_{j,k})^2$	Determines the contents of the speckle in the image. A lower variance gives a smoother image.
Noise Standard Deviation (NSD)	$NSD = \dfrac{SORT((\sum_{j=1}^{M}\sum_{k=1}^{N}(X_{j,k}-NMV)^2)}{MN}$ where $NMV = \dfrac{\sum_{j=1}^{M}\sum_{k=1}^{N}X_{j,k}}{MN}$	Finds the content of the speckle noise in the image. Small NSD value represents a clear image.
Effective Number of Looks (ENL)	$ENL = \dfrac{[NMV]^2}{[NSD]^2}$	Measure of the statistical fluctuations introduced by speckle. A large ENL value represents better quantitative performance of the despeckle filter.
Geometric Average Error (GAE)	$GAE = \left(\prod_{j=1}^{M}\coprod_{k=1}^{N}\sqrt{X_{j,k}-X'_{j,k}}\right)^{\frac{1}{MN}}$	Measure the information between the original and the despeckled image
Figure of Merit (FOM)	$FOM = \dfrac{1}{\max(N_e,N_i)}\sum_{j=1}^{N}\dfrac{1}{1+d_j^2\alpha}$	Measure the performance of edge preservation of the image
Mean Structure Similarity Index Map (MSSIM) and Structure similarity index map (SSIM)	$MSSIM = \dfrac{1}{MN}\sum_{j=1}^{M}\sum_{K=1}^{N}SSIM[(X_{j,k}),(X'_{j,k})]$ where $SSIM(X,X') = \dfrac{(2\mu_X\mu_{X'}+C_1)(2\sigma_{XX'}+C_2)}{(\mu_X^2+\mu_{X'}^2+C_1)(\sigma_X^2+\sigma_{X'}^2+C_2)}$	MSSIM and SSIM are used to compare luminance, contrast and structure between the original and denoised images. The MSSIM value should be closer to unity for optimal measure of similarity.

IV. Implementation of Despeckle Algorithm and Results

In this study, the cumulative speckle reduction (CSR) algorithm comprising of nine traditional single scale spatial adaptive filters, one Multiscale filter, two diffusion filters of different iteration levels, and twenty one qualitative metrics estimation, has been developed in the MATLAB7.1 environment. More than 200 digital ultrasound B-scan images of organs like kidney, choroids, abdomen and liver were obtained for several cases from the GE healthcare ultrasound machine (Model: VIVID7). The CSR algorithm was tested in all the 200 digital B-scan images, which provided the despeckle output images of the nine spatial filters, one multiscale filter in a single iteration with the despeckle output images of two diffusion filters (SRAD and PMAD) of different iterations, and twenty one performance metrics with execution time calculation in a single trial. Due to space limitation, the original and despeckled B-scan images outputs of all the twelve filters and their respective SSIM image outputs of the kidney are given in fig.3 and fig.4, respectively. The graphical representation of the performance metrics of all the filters with their execution time are given in the fig.5. Further, the various performance metrics calculated for the standard and multiscale filter are given in Table II. Similarly, the metrics for the SRAD and PMAD are given in table III and IV, respectively. From the visual inspection of the despeckled images and careful inspection of the metrics calculated, the following interpretations have been arrived.

1. Frost and Median filters slightly improve the information of the edges, but the Lee filter improves the ability of preserving the edges.
2. Kuan filter is relatively better than the Lee filter.
3. Performance of the frost filter is similar to that of the enhanced Lee filter.
4. Kuan and Frost filters despeckle the image to some extent. But, it can also be found from the metrics that Frost filter is better than the Kuan filter for speckle reduction, since it has higher SNR,PSNR, SC, and CoC values and lower MSE and RMSE values than Kuan filter.
5. Enhanced Frost filter improves the performance of the frost filter and the performance of the enhanced frost filter is better than the enhanced Lee filter.
6. Gamma MAP filter performance is similar to the Kuan filter.
7. Homomorphic filter sharpens the image and flattens the speckle variation since it has very low PSNR and

high MD values. The FoM values are very low compared to the other filters.

8. Wiener is the better approach as per as spatial filters are concerned, since it has performance metrics comparable with the outperformed SRAD filter. But SRAD has exceptional performance than Wiener in terms of metrics like AD, MD, MSE, RMSE, NAE, IV and visual inspection.
9. PMAD filter in B-scan images enhances the speckle noise rather than suppressing it. The parameters like PSNR, SC, NCC, IV clearly depicts that the PMAD filter is not an efficient filter for the ultrasound images. Also, the image quality index Q and SSIM decreases as the iteration value increases which shows that the image is distorted rather than enhanced to a great extend.
10. The SRAD suppresses the speckle noise to a great extend. The performance metrics AD, MSE, RMSE, MD, NAE, SC, ASNR, and NSD increases as the iteration value increases. Conversly, the values of PSNR, CoC, NCC, Q, SI, IV, ENL, and MSSIM decreases as the iteration increases. The values of the SNR, NMSE, CNR increases when the iteration value increases. The value of the FoM increases when the value of the iteration decreases. As the iteration value in SRAD increases, the speckle noise decreases. But, it should be noted that this also blurs the image. So, the optimum values of iteration found in this study is in the range of 2-9. Thus, all the spatial and diffusion filter performance were compared and tested experimentally for various digital ultrasound B-scan images interms of performance metrics. From the filtered output images and the performance metrics it has been verified that the SRAD filtering approach is performing better than the traditional spatial filters and is an optimal filtering approach for speckle reduction from B-scan ultrasound images.
11. Finally, the Wavelet filter performs little bit equal performance to the SRAD filter, since the performance metric values are as close to the SRAD filter.

V. Conclusion

In this paper, we have developed a cumulative speckle reduction (CSR) algorithm for nine spatial, one multiscale, two diffusion type filters, and twenty one performance metrics with execution time calculation for the estimation of the optimum despeckle filter for real-time application. The algorithm was developed in MATLAB 7.1 and tested in more than 200 ultrasound B-scan images of four different organs viz liver, abdomen, choroids kidney and Liver. In all these images, the algorithm performs well and produces performance-measuring metrics in terms of the image content within the limited range, consistently. Further, the algorithm generates all the twelve filter outputs as well as twenty one performance metrics in single/multiple iterations in a single trial. Based on the results obtained and the visual inspection of the despeckled ultrasound B-scan image outputs, we conclude that the SRAD and multiscale wavelet filter exhibits a highly efficient speckle noise reduction with the ability to preserve and even enhance the edges of the images in comparison with the other standard single scale spatial adaptive filters. Moreover, the SRAD filter and wavelet filter are able to generate B-scan images with better quality for feature extraction and excels over the traditional filters in terms of speckle reduction, edge preservation and image clarity.

Acknowledgment

We acknowledge the help extended by Prof. Dr. S. Thanikachalam, Chairman, Cardiac Care Centre, SRMC Hospital, Chennai for providing various ultrasound B-scan images to conduct this study. Also, we record the financial assistance provided by Tamilnadu State Council for Science Technology (TNSCST), Chennai to carry out this work

References

[1] Thomas L. Szabo, "Diagnostic Ultrasound imaging, Academic Press Series in Biomedical Engineering," Elsevier Academic Press, 2004.
[2] Kayvan Najarian, and Robert Splinter, "Biomedical Signal and image processing, Taylor and Francis publications," pp.333-364, 2006.
[3] Chris Guy, and Dominic ffytche, "An Introduction to the principles of medical imaging," Revised edition, Imperial College Press, pp.267-294, 2005.
[4] William R. Hendee, and E. Russell Ritenour, "Medical Imaging Physics," fourth edition, John Wiley and Sons, Inc., Publication, pp.317-338, 2002.
[5] Streve Webb, "The Physics of Medical imaging, Medical Science Series," Taylor and Francis Group, pp.319-377, 1988.
[6] Robert F. Wagner, Stephen W. Smith, John M. Sandrik, and Hector Lopez, "Statistics of Speckle in Ultrasound B- Scans," IEEE Trans. on Sonics and Ultrasonics, Vol. 30, no. 3, pp.156-163, May 1983.
[7] J.W. Goodman, "Some Fundamental Properties of Speckle," Journal of Optical Society of America, Vol.66, No.11, pp.1145-1150, November 1976.
[8] Christoph B. Burckhardt, "Speckle in Ultrasound B-Mode Scans," IEEE Trans. on Sonics and Ultrasonics, Vol.25, No.1, pp.1-6, 1978.
[9] Mustafa Karaman, M. Alper Kutay, and Gozde Bozdagi, "An Adaptive Speckle Suppression Filter for Medical Ultrasonic Imaging," IEEE Trans. On Medical Imaging, Vol. 14, No.2, pp.283-292, 1995.
[10] Victor S. Frost, Josephine Abbott stiles, K. S. Shanmugan, and Julian C. Holtzman, "A Model for Radar Images and Its Application to Adaptive Digital Filtering of Multiplicative Noise," IEEE Trans. on Pattern Analysis and Machine Intelligence, Vol. PAMI-4, No.2, pp.157-166, March 1982.
[11] Alin Achim, Anastasios Bezerianos and Panagiotis Tsakalides, "Novel Bayesian Multiscale Method for Speckle Removal in Medical Ultrasound Images," IEEE Trans. on Medical Imaging, Vol. 20, No. 8, pp.772-783, August 2001.
[12] J. S. Lee, "Digital Image Enhancement and Noise Filtering by Use of Local Statistics," IEEE Trans. on Pattern Analysis and Machine Intelligence, Vol. PAMI-2, No. 2, pp.165-168, March 1980.
[13] J. S. Lee, "Refined filtering of image noise using local statistics," Computer Vision, Graphics, and Image Processing. Vol.15, pp.380-389, 1981.
[14] D. T. Kuan, A. A. Sawchuk, T.C. Strand, and P. Chavel, "Adaptive restoration of images with speckle," IEEE Trans. on Acoustics, Speech and Signal Processing, Vol. ASSP-35, No.3, pp.373-383, March1987.
[15] Anil K. Jain, "Fundamentals of Digital Image Processing," first edition, Prentice-Hall, Inc, 1989.
[16] Stian Solbo and Torbjorn Eltoft, "Homomorphic Wavelet-Based Statistical Despeckling of SAR Images," IEEE Trans. on Geoscience and Remote Sensing, Vol. 42, No. 4, pp.711-721, April 2004.
[17] S.Kalaivani Narayanan and R.S.D. Wahidabanu, "A View on Despeckling in ultrasound imaging," International Journal of Signal Processing.Image Processing and Pattern Recognition, Vol.2, No.3, September 2009.
[18] Zhanghao Shi, and KoB. Fang, " A Comparison of Digital Speckle Filters,"Canadian Crown, 0-7803-1497-2194, pp.2129-2133.
[19] Nadia Souag, "Speckle Reduction in Echocardiographic Images," 14th European signal processing conference (EUSIPCO 2006) Proceeding, Florence, Italy, Sept 4-8, 2006.

[20] Armand Loper, Ridha Touzi, and N.Nezry, "Adaptive Speckle Filters and Scene Heterogeneity," IEEE Trans. On Geoscience and Remote Sensing, Vol.28,No.6, pp.992-1000, November 1990.
[21] Raman Maini, and Himanshu Aggarwal, "Performance Evaluation of Various Speckle Noise Reduction Filters on Medical Images," International Journal of Recent Trends in Engineering, Vol.2, No.4, pp.22-25, November 2009.
[22] Rafael C. Gonzalez, and Richard E. Woods, "Digital Image Processing," Third Edition, Pearson Education, 2008.
[23] Christos P. Loizou, Constantinos S. Pattichis, Christodoulos I. Christodoulou, Robert S. H. Istepanian, Marios Pantziaris, and Andrew Nicolaides, "Comparative Evaluation of Despeckle Filtering In Ultrasound Imaging of the Carotid Artery," IEEE Trans. on Ultrasonics, Ferroelectrics, and Frequency control, Vol. 52, No.10, pp.1653-1669, October 2005.
[24] Karunesh K. Gupta, and Rajiv Gupta, "Despeckle and geographical feature extraction in SAR images by wavelet transform," ISPRS Journal of Photogrammetry and Remote Sensing, Vol. 62, pp.473-484, July 2007.
[25] S.G. Mallat, "A theory for multiresolution signal decomposition: the wavelet representation," IEEE Trans. On Pattern Analysis and Machine Intelligence, Vol.11, No.7, pp.674-693, July 1989.
[26] S.G. Mallat, "Multifrequency channel decomposition of images and wavelets models," IEEE Trans. On Acoustics, speech, and Signal Processing, Vol.37, No.12, pp.2091-2110, December 1989.
[27] Byeongcheol Yoo, and Toshihiro Nishimura, "A Study of Ultrasound Images Enhancement using Adaptive Speckle Reducing Anisotropic Diffusion," IEEE International Symposium on Industrial Electronics (ISIE 2009) July 5-8, Seoul Olympic Parktel, Seoul, Korea, pp.581-585, 2009.
[28] Yongjian Yu, and Scott T. Acton, "Speckle Reducing Anisotropic Diffusion," IEEE Trans. on Image Processing, Vol. 11, No.11, pp.1260-1270, November 2002.
[29] P. Perona and J. Malik, "Scale space and edge detection using anisotropic diffusion," IEEE Trans. on Pattern Analysis and Machine Intelligence, Vol.12, No.7, pp. 629–639, JULY 1990.
[30] Jesse S. Jin, Yung Wang, and John Hiller, "An Adaptive Nonlinear Diffusion Algorithm for Filtering Medical Images," IEEE Trans. on Information Technology in Biomedicine, Vol. 4, No.4, pp. 298-305, December 2000.
[31] Khaled Z. Abd-Elmoniem, Abou-Bakr M. Youssef, and Yasser M. Kadah, "Real-Time Speckle Reduction and Coherence Enhancement in Ultrasound imaging via nonlinear anisotropic diffusion," IEEE Trans. on Biomedical Engineering, Vol.49, No.9, pp.997-1014, September 2002.
[32] C. I. Christodoulou, C. Loizou, C. S. Pattichis, M. Pantziaris, E. Kyriakou, M. S. Pattichis, C. N. Schizas, and A. Nicolaides, "Despeckle filtering in ultrasound imaging of the carotid artery," Proceedings of the second joint EMBS/BMES Conference, Texas, USA, and pp.1027-1028, October 23-26, 2002.
[33] Sonja Grgic, Mislav Grgic, and Marta Mrak, "Reliability of objective picture quality measures," Journal of Electrical Engineering, Vol.55, No.1-2, pp.3-10, 2004.
[34] Ahmet M. Eskicioglu, and Paul S. Fisher, "Image quality measures and their performance," IEEE Trans. on Communications, Vol.43, No.12, pp.2959-2965, Dec.1995.
[35] Zhou Wang and Alan C. Bovik,"A Universal image quality index,"IEEE Signal Processing Letters, Vol.9, pp.81-84, March 2002.
[36] Rajeev Srivastava J.R.P Gupta, and Harish Parthasarthy, "Comparison of PDE based and other techniques for speckle reduction from digitally reconstructed holographic images," Journal of Optics and Lasers in Engineering, ELSEVIER, Vol.48, pp.626-635, 2010.
[37] G.Padmavathi, P.Subashini, M.Muthu Kumar, and Suresh Kumar Thakur, " Comparison of Filters used for underwater Image Pre-Processing," International Journal of Computer Science and Network Security, Vol.10, No.1, pp.58-65, January 2010.
[38] Zhou Wang, Alan Conrad Bovik, Hamid Rahim Sheikh, and Eero P. Simoncelli, "Image Quality assessment: from Error visibility to structural similarity," IEEE Trans. on Image Processing, Vol.13, No.4, pp.600-612, April 2004.
[39] Ismail Avcibas, Bulent Sankur, and Khalid Sayood, "Statistical evaluation of Image quality measures," Journal of Electronic Imaging, Vol.11, No.2, pp.206-223, April 2002.
[40] T.Ratha Jeyalakshmi, and K.Ramar, "A Modified method for Speckle Noise Removal in ultrasound medical images," International Journal of computer and Electrical Engineering (IJCEE), Vol.2, No.1, pp.54-58, February 2010.
[41] A.Miranda Neto, L.Rittner, N.Leite, D.E.Zampieri, R.Lotufo, and A.Mendeleck, "Pearson's Correlation Coefficient for Discarding Redundant Information in Real Time Autonomous Navigation System," 16th IEEE International Conference on Control Applications, Proceedings pp.426-431, Singapore, 4-3 October 2007.
[42] S.Gupta, L.Kaur, R.C.Chauhan, and S.C.Saxena, "A Versatile Technique for visual enhancement of medical ultrasound image," Journal of Digital Signal Processing, ELSEVIER, Vol.17, pp.542-560, January 2007.
[43] V.V.K.D.V. Prasad , P.Siddaiah, and B.Prabhakara Rao, "A New Wavelet Based Method for Denoising of biological signals," International Journal of Computer Science and Network Security, Vol.8, No.1, pp.238-244, January 2008.
[44] Fan Zhang, Yang Mo, Yoo, Liang Mong Koh, and Yongmin kion, " Nonlinear Diffusion in Laplacian Pyramid Domain for Ultrasonic Speckle Reduction," IEEE Trans. On Medical Imaging, Vol.26, No.2, pp.200-211, February 2007.
[45] Chen Jie, Zhu Jing, Li Chunsheng, and Zhou Yinqing, " A Novel Speckle Filter for SAR images Based on information- Theoretic Heterogeneity Measurments," Chinese Journal of Aeronautics, Vol.22, pp.528-534, May 2009.
[46] S. Sudha, G.R Suresh, and R. Suknesh, "Speckle Noise Reduction in Ultrasound images By Wavelet Thresholding Based On Weighted Variance", International Journal of Computer Theory and Engineering, Vol. 1, No.1, PP 7-12,2009.

Mr. R. Sivakumar was born in the year 1980. He received his M.Sc., Physics degree from A.M. Jain College, University of Madras, in the year 2004. Currently he is pursuing Ph.D in Biomedical Image Processing in the Central Instrumentation and Service Laboratory, University of Madras, Guindy Campus, Chennai, Tamilnadu, India. He was awarded Tamilnadu State Council for Science and Technology (TNSCST) fellowship for doing his research work. His areas of interest are Medical image processing, and analysis. He is a member of the International Association of Computer Science and Information Technology (IACSIT).

Ms. M. K. Gayathri was born in Chennai during the year 1987. She received her M. Sc Physics degree in the year 2009 from Meenakshi College for Women, University of Madras. She just finished the M. Phil degree in Scientific Instrumentation from University of Madras, Chennai, India. Her research interests are in the area of medical image processing, and pattern recognition.

Dr. Damodaran Nedumaran was born in the year 1965. He obtained his M. Sc degree in Physics from Bharathidasan University and M. Phil., and Ph. D. in Scientific Instrumentation from University of Madras. He was awarded the Tamilnadu Junior Research Fellowship (TNJRF) for pursuing his research degree course. He started his professional carrier as Research & Development Scientist at Ozonetek Limited, Chennai. He has developed indigenous, novel and economical circuits for ozone generation and control applications. In the year 2000, he joined as Assistant Professor, in the Department of Central Instrumentation & Service Laboratory, University of Madras. Currently he is working as Assistant Professor (Stage 2) in the same department. He has published many papers on various aspects of instrumentation in reputed national and international journals. He has coordinated and attended many conferences, seminars and symposium in the national as well as international level. He has been life member and member of many professional association of international repute viz., IEEE, IETE, ISOI, IPA, MSI, and IACSIT. He has been teaching various instrumentation subjects at the Post Graduate and M. Phil level. In addition, he has been involved in guiding research scholars and handling research projects in the area of biomedical signal and image processing, biometric image processing, ozone generation and application techniques, Virtual Instrumentation techniques, and MEMS based sensor design.

TABLE II CALCULATED PERFORMANCE METRICS OF THE VARIOUS DESPECKLING FILTERS IMPLEMENTED IN THE CSR ALGORITHM FOR KIDNEY B-SCAN IMAGE

Performance Metrics	Frost	Lee	Kuan	Enhanced Frost	Enhanced Lee	Median	Gamma MAP	Wiener	Homo morphic	Wavelet
AD	0.108	0.427	0.433	0.283	0.526	0.243	0.459	0.035	96.316	0.003
MSE	44.670	121.113	114.257	42.189	44.773	45.671	130.913	23.444	1.33E+6	20.776
RMSE	6.683	11.005	10.689	6.495	6.691	6.758	11.441	4.841	115.676	4.558
PSNR	31.630	27.298	28.361	33.259	31.783	31.534	29.218	34.430	6.865	35.116
MD	114	232	213	104	116	169	246	32	253.195	56
NAE	0.037	0.049	0.037	0.029	0.034	0.033	0.051	0.033	0.983	0.037
NMSE	1.22E-6	1.90E-5	1.83E-5	1.28E-6	1.27E-6	6.16E-6	1.97E-5	1.31E-7	9.67E-1	6.76E-10
SNR	0.186	0.142	0.187	0.216	0.118	0.099	0.143	0.069	52.885	0.156
SC	1.029	1.016	1.128	1.114	1.009	1.010	1.114	1.005	5.24E+6	0.987
COC	0.994	0.983	0.985	0.986	0.992	0.994	0.986	0.997	0.964	1.008
NCC	0.994	0.967	0.988	0.989	0.997	0.993	0.992	0.996	0.012	1.016
Q	0.873	0.825	0.836	0.863	0.873	0.854	0.843	0.851	0.000	0.989
CNR	1.33E-5	5.18E-5	5.26E-5	1.41E-5	1.45E-5	2.98E-5	5.24E-5	4.34E-6	2.33E-2	4.73E-7
SI	6.45E-6	6.45E-6	6.45E-6	6.45E-6	6.45E-6	6.45E-6	6.37E-6	6.45E-6	6.45E-6	6.45E-6
ASNR	1.54E+5	1.54E+5	1.54E+5	1.67E+5	1.54E+5	1.54E+5	1.54E+5	1.54E+5	1.54E+5	1.54E+5
IV	4.12E+3	4.12E+3	4.12E+3	4.12E+3	4.12E+3	4.12E+3	4.12E+3	4.12E+3	4.12E+3	4.12E+3
NSD	9.73E+8	9.73E+8	9.73E+8	9.73E+8	9.73E+8	9.73E+8	9.73E+8	9.73E+8	9.73E+8	9.73E+8
ENL	1.01E-14	1.01E-14	1.01E-14	1.01E-14	1.01E-14	1.01E-14	1.01E-14	1.01E-14	1.01E-14	1.01E-14
GAE	0.00	0.00	0.00	0.00	0.00	0.00	0.00	0.00	0.00	0.00
FOM	0.5253	0.5312	0.5217	0.5213	0.5112	0.5004	0.5312	0.5523	0.1057	0.5613
MSSIM	0.913	0.884	0.889	0.904	0.905	0.901	0.906	0.908	0.0396	0.998
Elapsed time	11.438	15.357	15.119	13.719	14.162	0.069	16.113	0.731	1.860	5.114

TABLE III CALCULATED PERFORMANCE METRICS OF SRAD FILTER FOR DIFFERENT ITERATIONS IN KIDNEY B-SCAN IMAGE

Performance Metrics	SRAD (I=2)	SRAD (I=3)	SRAD (I=4)	SRAD (I=5)	SRAD (I=6)	SRAD (I=7)	SRAD (I=8)	SRAD (I=9)
AD	0.002	0.005	0.007	0.014	0.017	0.023	0.029	0.032
MSE	16.301	35.464	60.452	86.877	113.130	136.084	157.881	177.295
RMSE	4.037	5.955	7.775	9.321	10.636	11.665	12.565	13.315
PSNR	36.008	32.632	30.316	28.741	27.594	26.792	26.147	25.643
MD	47	65	199	199	253	253	253	253
NAE	0.026	0.0387	0.054	0.064	0.069	0.075	0.081	0.085
NMSE	7.10E-10	3.34E-9	6.36E-9	2.14E-8	3.29E-8	5.97E-8	9.19E-8	1.11E-7
SNR	0.118	0.171	0.217	0.261	0.303	0.341	0.376	0.408
SC	1.008	1.011	1.015	1.018	1.024	1.023	1.026	1.028
COC	0.998	0.995	0.992	0.989	0.986	0.983	0.981	0.978
NCC	0.995	0.992	0.991	0.987	0.985	0.983	0.985	0.979
Q	0.952	0.886	0.792	0.682	0.589	0.519	0.465	0.421
CNR	3.21E-7	7.01E-7	9.71E-7	1.77E-6	2.23E-6	3.01E-6	3.75E-6	4.16E-6
SI	6.45E-6	6.45E-6	6.45E-6	6.45E-6	6.45E-6	6.45E-6	6.45E-6	6.45E-6
ASNR	1.54E+5	1.54E+5	1.54E+5	1.54E+5	1.54E+5	1.54E+5	1.54E+5	1.54E+5
IV	4.12E+3	4.12E+3	4.12E+3	4.12E+3	4.12E+3	4.12E+3	4.12E+3	4.12E+3
NSD	9.73E+8	9.73E+8	9.73E+8	9.73E+8	9.73E+8	9.73E+8	9.73E+8	9.73E+8
EN	1.01E-14	1.01E-14	1.01E-14	1.01E-14	1.01E-14	1.01E-14	1.01E-14	1.01E-14
GAE	0.00	0.00	0.00	0.00	0.00	0.00	0.00	0.00
FOM	0.5769	0.5714	0.5647	0.5609	0.5487	0.5312	0.5234	0.5214
MSSIM	0.964	0.919	0.864	0.799	0.748	0.711	0.684	0.664
Elapsed time	0.999	1.008	1.235	1.537	1.822	2.147	2.422	2.725

TABLE IVCALCULATED PERFORMANCE METRICS OF PMAD FILTER FOR DIFFERENT ITERATIONS IN THE KIDNEY B-SCAN IMAGE

Performance Metrics	PMAD (I=5)	PMAD (I=7)	PMAD (I=10)	PMAD (I=13)	PMAD (I=15)	PMAD (I=17)	PMAD (I=20)	PMAD (I=25)
AD	6.911	9.034	11.928	14.574	16.237	17.835	20.129	23.732
MSE	100.192	166.834	282.791	413.862	507.981	606.646	761.983	1037.1
RMSE	10.009	12.916	16.816	20.343	22.538	24.632	27.604	32.204
PSNR	28.122	25.907	23.616	21.962	21.072	20.301	19.311	17.972
MD	52	74	87	103	116	125	133	147
NAE	0.078	0.092	0.121	0.148	0.165	0.182	0.205	0.242
NMSE	0.004	0.008	0.014	0.022	0.027	0.033	0.042	0.058
SNR	-0.326	-0.433	-0.572	-0.692	-0.762	-0.826	-0.912	-1.025
SC	0.888	0.857	0.817	0.783	0.764	0.745	0.725	0.684
COC	0.994	0.991	0.986	0.980	0.976	0.972	0.966	0.955
NCC	1.059	1.077	1.101	1.122	1.135	1.148	1.165	1.192
Q	0.880	0.825	0.751	0.688	0.651	0.618	0.575	0.516
CNR	8.06E-4	1.21E-3	1.41E-3	1.61E-3	1.81E-3	2.04E-3	2.21E-3	2.54E-3
SI	6.45E-6	6.45E-6	6.45E-6	6.45E-6	6.45E-6	6.45E-6	6.45E-6	6.45E-6
ASNR	1.54E+6	1.54E+5	1.54E+5	1.54E+5	1.54E+5	1.54E+5	1.54E+5	1.54E+5

ISSN: 1793-8236

IV	4.12E+3	4.12E+3	4.12E+3	4.12E+3	4.12E+3	4.12E+3	4.12E+3	4.12E+3
NSD	9.73E+8	9.73E+8	9.73E+8	9.73E+8	9.73E+8	9.73E+8	9.73E+8	9.73E+8
ENL	1.01E-14	1.01E-14	1.01E-14	1.01E-14	1.01E-14	1.01E-14	1.01E-14	1.02E-14
GAE	0.00	0.00	0.00	0.00	0.00	0.00	0.00	0.00
FOM	0.5324	0.5316	0.5289	0.5236	0.5173	0.5146	0.5014	0.5009
MSSIM	0.908	0.831	0.801	0.749	0.719	0.693	0.659	0.615
Elapsed time	1.521	0.893	1.242	1.575	1.822	2.038	2.389	2.957

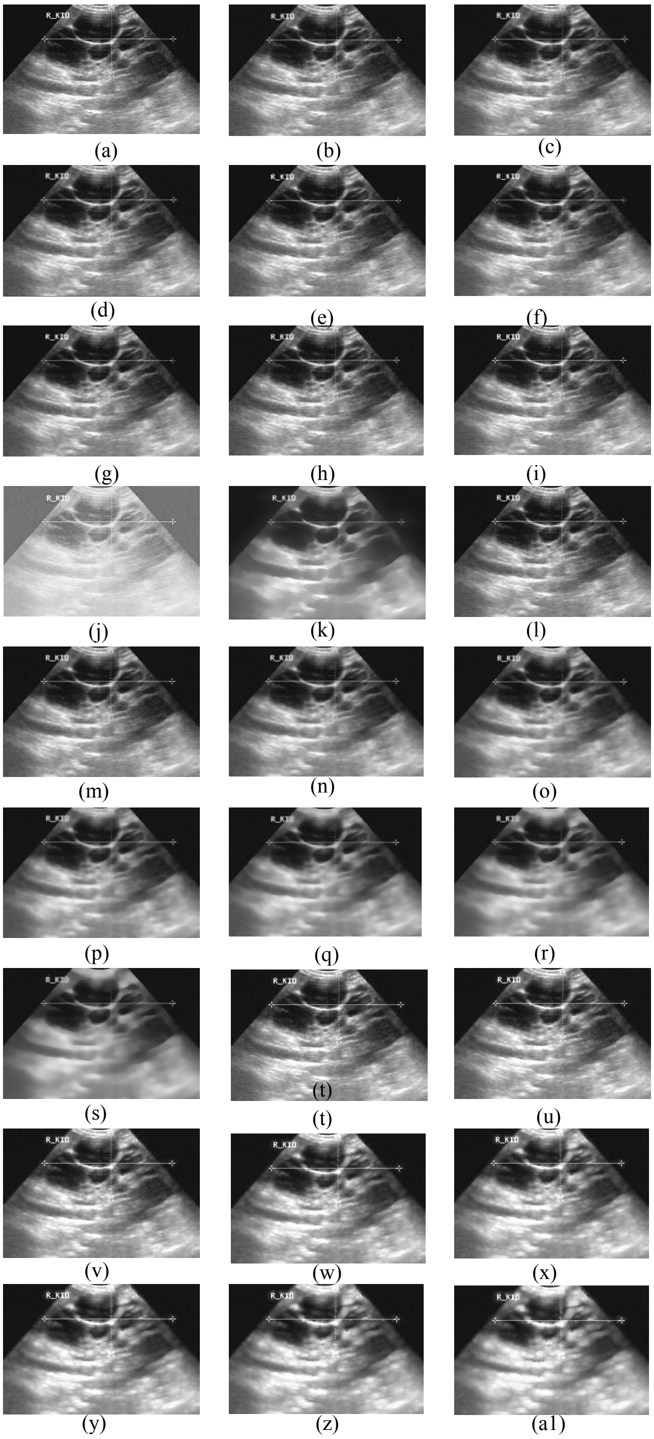

Fig. 3 View of the original and despeckled kidney images (a) Original Image (b) Frost filtered image (c) Lee filtered image (d) Kuan filtered image (e) Enhanced Frost filtered image (f) Enhanced Lee filtered image (g) Median filtered image (h) Gamma filtered image (i) Wiener filtered image (j) Homomorphic filtered image (k) Wavelet filtered image (l) SRAD (I=2) filtered image (m) SRAD (I=3) filtered image (n) SRAD (I=4) filtered image (o) SRAD (I=5) filtered image (p) SRAD (I=6) filtered image (q) SRAD (I=7) filtered image (r) SRAD (I=8) filtered image (s) SRAD (I=9) filtered image (t) PMAD (I=5) filtered image (u) PMAD (I=7) filtered image (v) PMAD (I=10) filtered image (w) PMAD (I=13) filtered image (x) PMAD (I=15) filtered image (y) PMAD (I=17) filtered image (z) PMAD (I=20) filtered image (a1) PMAD (I=25) filtered image

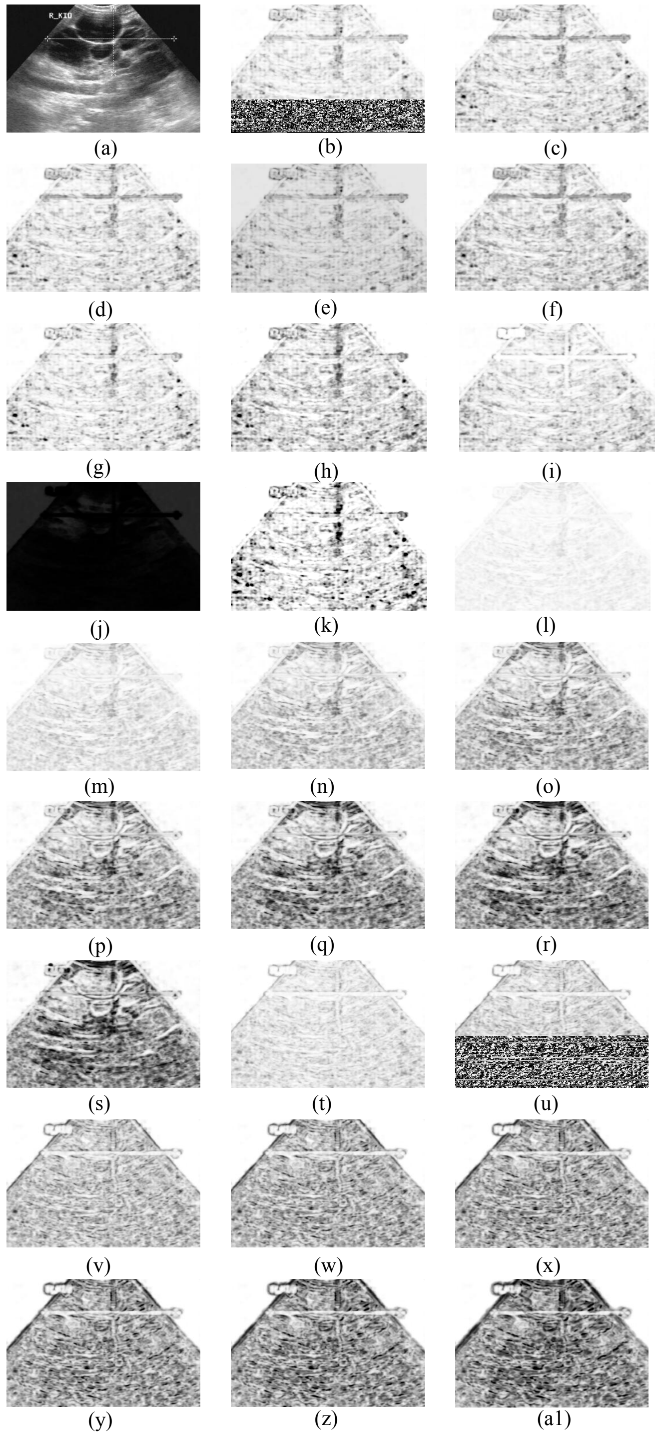

Fig. 4 View of the original and SSIM factor images of the kidney (a) Original Image (b) Frost filtered image (c) Lee filtered image (d) Kuan filtered image (e) Enhanced Frost filtered image (f) Enhanced Lee filtered image (g) Median filtered image (h) Gamma filtered image (i) Wiener filtered image (j) Homomorphic filtered image (k) Wavelet filtered image (l) SRAD (I=2) filtered image (m) SRAD (I=3) filtered image (n) SRAD (I=4) filtered image (o) SRAD (I=5) filtered image (p) SRAD (I=6) filtered image (q) SRAD (I=7) filtered image (r) SRAD (I=8) filtered image (s) SRAD (I=9) filtered image (t) PMAD (I=5) filtered image (u) PMAD (I=7) filtered image (v) PMAD (I=10) filtered image (w) PMAD (I=13) filtered image (x) PMAD (I=15) filtered image (y) PMAD (I=17) filtered image (z) PMAD (I=20) filtered image (a1) PMAD (I=25) filtered image

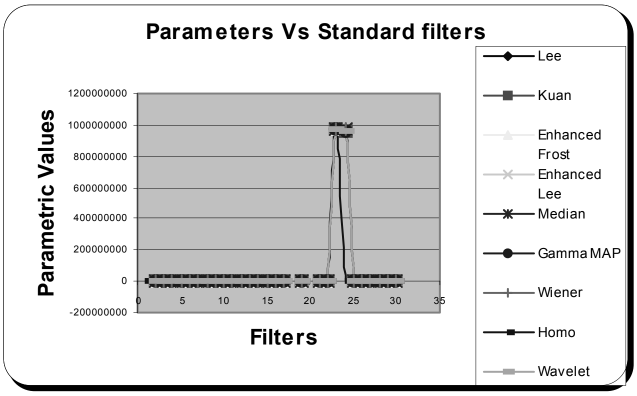

(a)

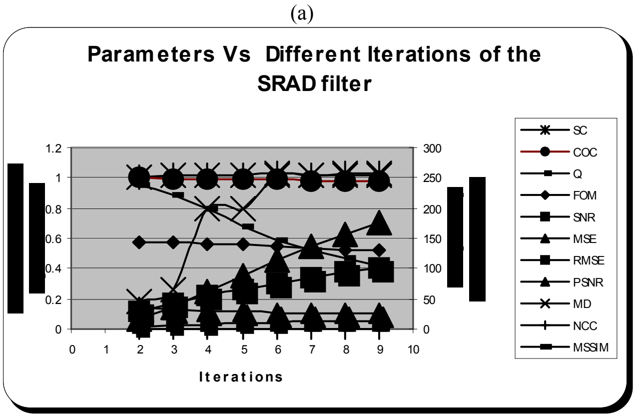

(b)

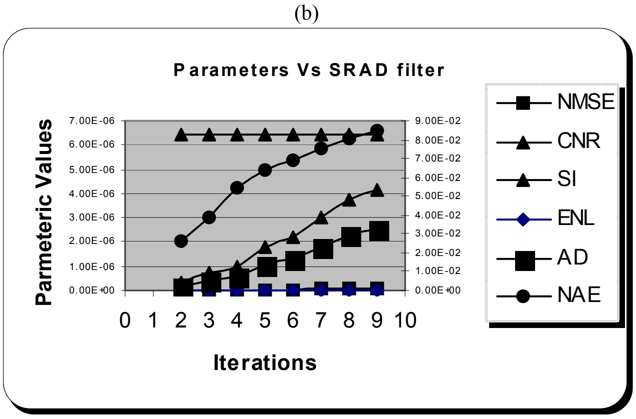

(c)

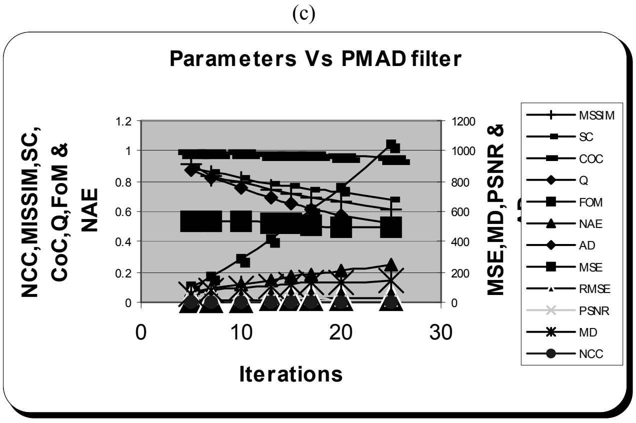

(d)

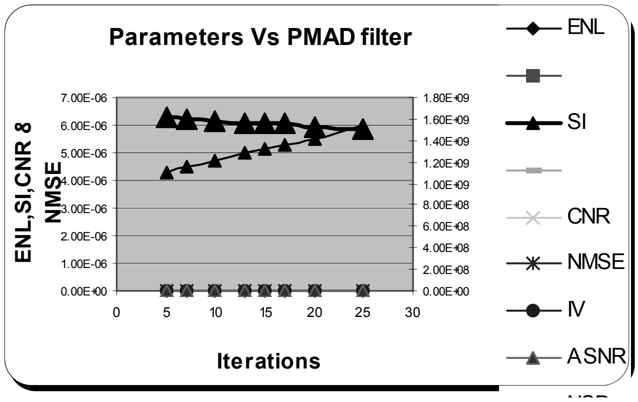

(e)

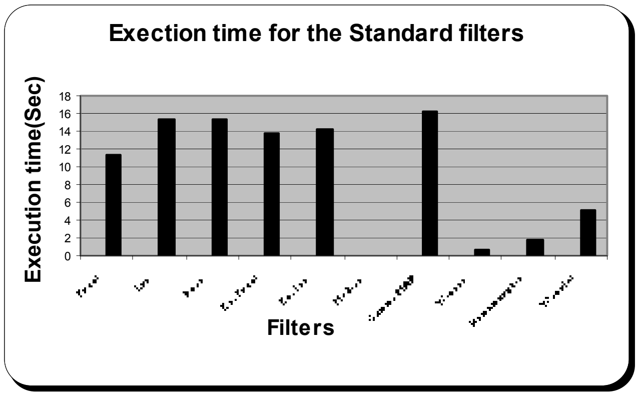

(f)

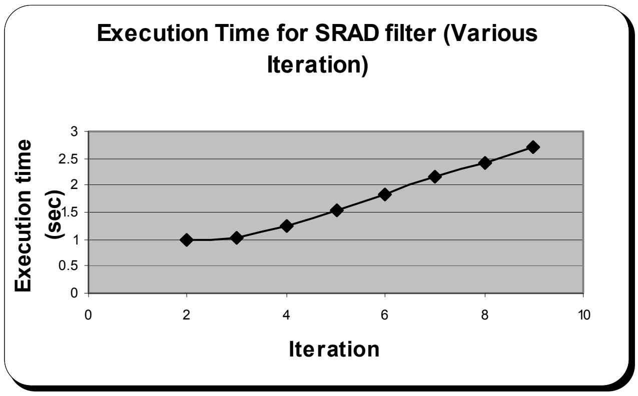

(g)

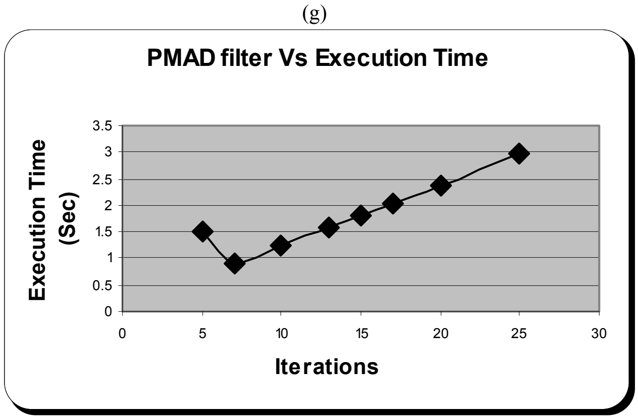

(h)

Fig.5 Graphical Representation of the performance metrics of the kidney B-Scan images (a) Standard filter (b) & (c) SRAD filter (d) & (e) PMAD filter (f) Execution time comparison of standard filters (g) Execution time comparison of SRAD filter for different iterations (h) Execution time comparison of PMAD filter for different iterations